# DESIGN AND TESTING OF AN AUTOMATIC CONTROL SYSTEM FOR TOPSOIL STRIPPING OF FRITILLARIA USSURIENSIS MAXIM. BASED ON MACHINE VISION

1

# 基于机器视觉的平贝母表土剥离自动控制系统设计与试验

Ren-jie XIA 1), Yi-xin LIN 1), Kai-chun ZHANG 1), Shu-juan YI 1), Jiang-SONG\*1)

<sup>1)</sup>College of Engineering, Heilongjiang Bayi Agricultural University, Daqing/P. R. China *Tel:* +86-459-13945603348; *E-mail:* songjiang\_770313@163.com; *Corresponding author:* Jiang-Song

DOI: https://doi.org/10.35633/inmateh-77-62

Keywords: Fritillaria ussuriensis Maxim; topsoil stripping; machine vision; automatic control system; response time

#### **ABSTRACT**

In this study, a machine-vision-based automatic control system for the topsoil stripping of Fritillaria ussuriensis Maxim. (FUM) was designed to address the problems of manual adjustment, low control accuracy, and response lag in stripping-depth control during FUM harvesting. An improved YOLOv5s-SA target detection algorithm was used to calculate FUM density and was deployed on the Jetson Nano edge-computing platform. Combined with a fuzzy control algorithm, it drives the servo electric cylinder to achieve dynamic depth adjustment of the scraping board. Test results showed that, after deploying the target detection algorithm on the edge AI device and accelerating it with TensorRT, the average inference time was 0.077 s, and the system response time was 0.26 s, meeting the real-time requirements of agricultural operations. Simulation results indicated that the average error between the stripping depth of the automatic control system and the preset depth was 3.72 mm, representing a 44.1% improvement compared with fixed-depth control. The average ideal stripping rate reached 54.96%, an improvement of 21.66% over the 33.3% achieved under fixed-depth control.

#### 摘要

针对平贝母收获中表土剥离深度依赖人工调节、控制精度低及响应滞后等问题,设计了一种基于机器视觉的平贝母表土剥离自动控制系统。采用改进的 YOLOv5s-SA 目标检测算法实现平贝母识别密度计算,并部署于Jetson Nano 边缘计算平台上,结合模糊控制算法驱动伺服电缸,实现刮土板的动态深度调节。所提出的控制系统试验结果表明,目标检测算法在边缘 AI 设备部署并经 TensorRT 加速后,识别平均推理耗时为 0.077 s,响应时间 0.26s,满足农业作业实时性要求。模拟试验结果表明,自动控制系统剥离深度与预铺设深度平均误差为 3.72 mm,相较固定深度控制改善 44.1%,平均剥离理想率为 54.96%。相比于固定深度控制理想剥离率 33.3%,提升了 21.66%。

#### INTRODUCTION

Fritillaria ussuriensis Maxim. (FUM), a member of the lily family, is a perennial herbaceous plant (Fig. 1) (Li et al., 2025). The medicinal and harvestable part is the underground bulb, which has an average diameter of 3–30 mm (Jiao et al., 2022). It has properties such as heat-clearing, cough relief, and phlegm resolution and is widely used in the production of traditional Chinese medicine preparations and health food (Yang et al., 2025). FUM is mainly distributed in the Xiao Xing'anling Mountains and Changbai Mountains in the three northeastern provinces. According to incomplete statistics, its cultivation area has reached 100,000 mu, with an annual economic output value of more than one billion yuan, and it has high economic value (An et al., 2024).

Ren-jie Xia, M.S. Stud. Eng.; Yi-xin Lin, M.S.; Kai-chun Zhang, M.S.; Shu-juan Yi, Prof., Ph.D.; Jiang-Song\*, Prof., Ph.D.

Fig. 1 - Distribution of FUM stems, leaves, and fruits

At present, (FUM) is mainly harvested through manual digging and mechanical two-stage operations, which are labor-intensive, inefficient, and highly sensitive to seasonal rainfall during the peak harvest season, often resulting in significant post-harvest losses (*Song et al., 2023*). To address this, Heilongjiang Bayi Agricultural University has developed a two-stage FUM harvester (Fig. 2) (*Song et al., 2015*), consisting of a topsoil stripping unit and a screening unit (*Song et al., 2017*). In the first stage, the stripper removes surface soil to expose and loosen the bulbs, followed by natural drying. In the second stage, the mixture is collected and screened to complete harvesting.

However, accurate control of stripping depth is critical (*Li et al., 2022*). Over-stripping increases energy consumption and bulb damage, while under-stripping leads to soil contamination, longer screening times, and higher impurity rates. Existing machines still rely on manual depth adjustments based on visual observation, which suffers from poor precision and delayed response. Therefore, achieving automated control of stripping depth is essential for improving harvesting efficiency and reducing bulb damage.





(a) Fig. 2 – Two-stage FUM harvester
(a) FUM topsoil stripper (b) FUM screening machine

With regard to the control of digging or stripping depth during the harvesting of underground fruits, current research by domestic and international scholars has mainly focused on obtaining surface characteristics through position sensors, ultrasonic waves, or ground pressure sensors and then achieving automatic depth limitation control through control algorithms such as fuzzy PID (Wang et al., 2025). Xiong et al., (2022), introduced a sensor + PLC + hydraulic system into a cassava harvester and adopted integrated separation fuzzy PID control to improve the harvester's performance. This system addressed issues such as unstable digging depth, cassava damage, high loss rates, and high energy consumption. Tao et al., (2021), designed an automatic depth control system for a tuber harvester. By using angle sensors to collect changes in the contour of the ridges, a dual-threshold dead zone control algorithm was employed to drive hydraulic cylinders and achieve real-time depth adjustment, effectively reducing tuber damage and missed harvesting rates. You et al., (2015), designed an ultrasonic distance measurement-based depth adjustment device for peanut harvesters, achieving real-time response control of digging depth. Dai et al., (2019), used an STM32 controller combined with a rotary encoder to construct a servo control system, achieving dynamic control of working depth. However, these methods are mainly based on surface features and cannot directly perceive crop information, resulting in "overdigging" or "underdigging" problems in field environments with uneven crop distribution or complex terrain. With the development of computer vision and deep learning, machine vision has gradually been applied to the field of agricultural automation. Ding et al., (2022), proposed an automatic digging depth control system for garlic combined harvesters based on YOLOv5. By using machine vision technology to calculate the length of garlic roots, the system drives the length of the electric push rod to achieve dynamic depth adjustment of the digging shovel.

Sang et al., (2024), designed a corn sowing depth consistency adjustment system based on a stereoscopic structured light camera, which can detect the trench depth in real time and drive an electronically controlled soil covering and compacting mechanism for adaptive adjustment, thereby reducing depth errors during the sowing process. Shi et al., (2024) used lidar technology to detect the cutting height of sugarcane harvesters in real time and combined displacement sensors to achieve closed-loop control, thereby improving adaptability to hilly terrain. In summary, most of the current research on limited depth digging technology focuses on peanuts and potatoes, while only mechanical structure research has been conducted on FUM harvesting.

On the basis of the above analysis, this study proposes a machine vision-based automatic control system for FUM topsoil stripping. The system uses an improved YOLOv5 target detection algorithm to identify changes in FUM density in the stripping area in real time and combines a servo mechanism to adjust the stripping depth automatically, thereby achieving automatic control of the depth of FUM topsoil stripping. This provides a theoretical reference for the development and application of FUM topsoil stripping machines.

#### **MATERIAL AND METHODS**

## Overall system structure and working principle

As shown in Fig. 3, the platform comprises five modules: a drive mechanism, image acquisition module, topsoil stripping device, control system, and human—machine interface. The drive mechanism adopts a DC motor chain drive with Hall sensors for real-time speed monitoring. The image acquisition module uses an adjustable camera mounted above the rear of the scraper to capture stripping area images. The stripping device consists of a screw-type servo electric cylinder linked to the scraper plate for dynamic depth adjustment. The control system integrates a host computer, running a target detection model to estimate FUM exposure density, and a subordinate controller that combines detection results with current depth data to execute fuzzy control and generate adjustment commands. The human—machine interface enables parameter setting, real-time display of operation status and stripping depth, and manual intervention. During operation, captured images are processed by the host computer, and the controller outputs pulse signals to regulate the scraper depth adaptively.

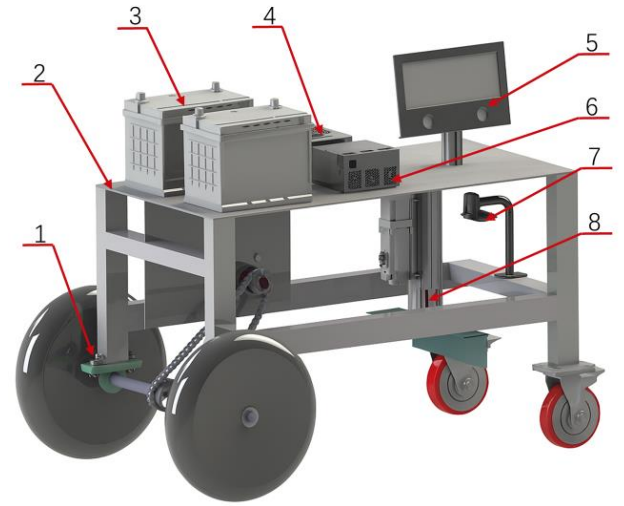


Fig. 3 - Topsoil stripping control system test platform

1. Vehicle speed detection device; 2. Work platform; 3. Power supply system; 4. Lower-level machine control system box; 5. Touchscreen; 6. Upper-level machine; 7. Camera; 8. Topsoil removal device.

#### Control system hardware design

The system's power module adopts a 24 V DC supply, with DC–DC converters providing 12 V and 5 V outputs to ensure voltage compatibility and stable operation across components. The image acquisition and processing module employs an NVIDIA Jetson Nano as the host controller, which integrates a 128-core CUDA GPU and 4 GB LPDDR4 memory. With support for TensorRT acceleration and USB 3.0 camera interface, it enables real-time image acquisition and target detection under low power consumption. Detection results are transmitted to the STM32F103ZET6 microcontroller via UART (115,200 bps), which executes control algorithms and generates pulse signals to drive a servo motor–actuated ball screw electric cylinder for scraper depth regulation. The control module also integrates Hall and displacement sensors for speed and position feedback. The execution module comprises a servo drive, electric cylinder, and scraping plate.

A touchscreen interface is used for system status display and parameter adjustment. Detailed hardware specifications are listed in Table 1. The hardware relationships among various systems are as shown in Fig. 4.

Detailed parameters of each equipment

Table 1

Part Name	Main Technical Parameters / Model Specifications		
24V power supply	24 V · 25 Ah		
DC-DC voltage regulator module	24 V→12 V,24 V→5 V		
Camera	1920 × 1080 @ 60 fps, USB 3.0 port		
Jetson Nano B01	4 GB LPDDR4, 128 CUDA cores (Maxwell)		
STM32F103ZET6	32-bit Cortex-M3,72 MHz, Flash 512 KB,UART(115 200 bps)		
Screw Type Servo Electric Cylinder	Stroke: 150 mm, screw guide 5 mm, thrust: 5000 N, speed: 50 mm/s, reduction ratio 4:1		
servo motor	Power: 400 W, rated speed: 3000 r/min, rated torque: 1.27 Nm		
Linear Displacement Sensors	Stroke 0-150 mm, output 0-5 V, resolution 0.05 mm		
DC Geared Motors	Power: 600 W, rated speed 60 r min-1		
Hall Velocity Sensors	60 ppr, NPN Open Collector Outputs		
13.3-inch touch screen	1920 x 1080, resistive touch, USB/HDMI communication		
scraper	Dimensions: 500 mm × 100 mm		

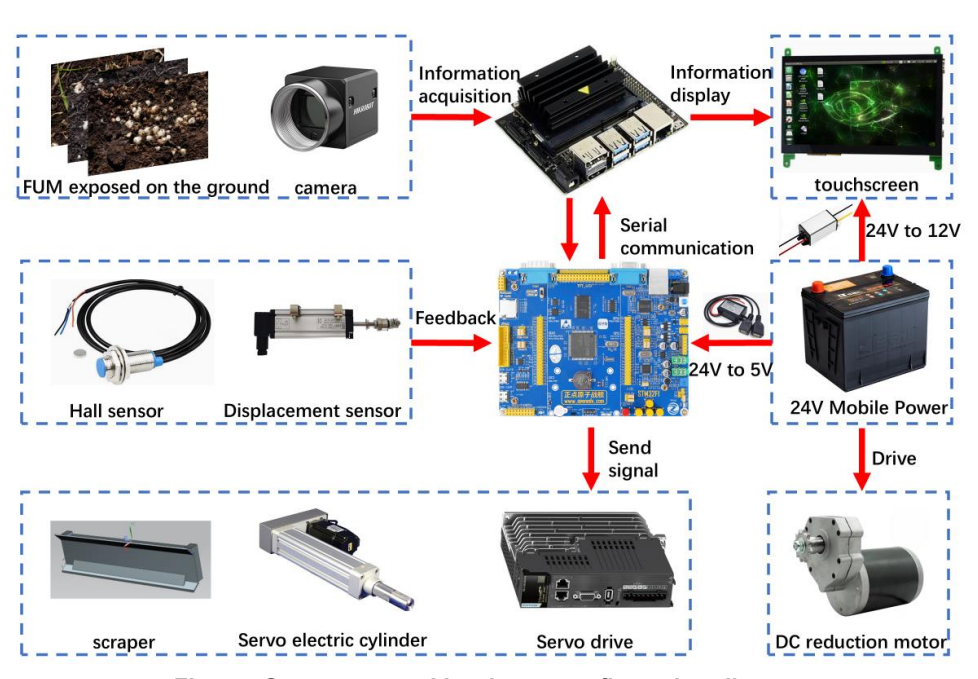


Fig. 4 – System control hardware configuration diagram

# Identification system design Data set production

To closely reflect real working conditions, image samples were collected from the FUM planting base in Hongxing, Yichun City, Heilongjiang Province, encompassing diverse scenarios such as varying lighting, occlusion, aggregation, and fragmentation (Fig. 5,  $a \sim f$ ). A total of 2,000 images (1280 × 960 resolution) were obtained to construct the FUM dataset.

The samples were augmented using affine transformation, mosaic enhancement, and histogram equalization (Fig. 5; g~h) to improve data diversity. The dataset was split into a training set (70%) and a validation set (30%), with the 1,400 training images expanded to 8,400 through augmentation to enhance the model's robustness to variations in target posture and scale (*Song et al., 2023*).

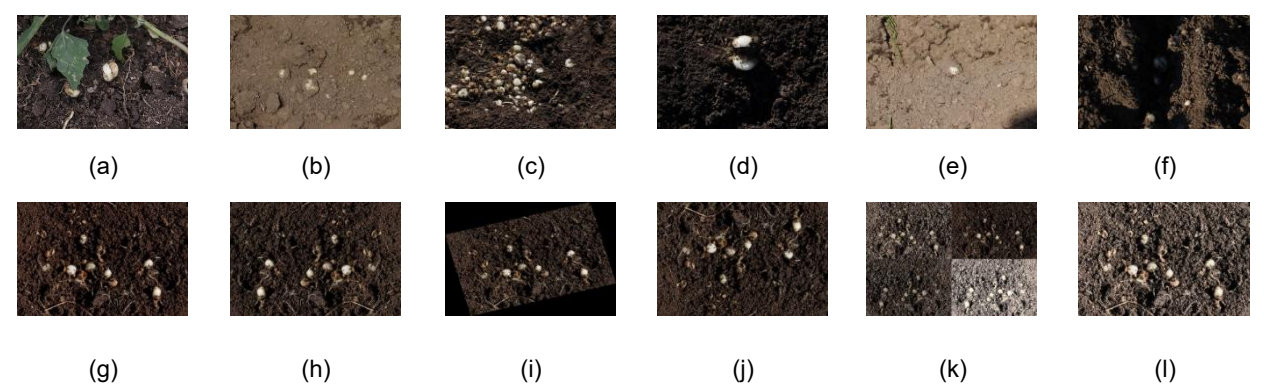


Fig. 5 - Examples of images of FUM in different environments and Effect of processing the dataset (a) Grass-covered FUM; (b) FUM covered with soil; (c) Multiple clusters of FUM; (d) Broken FUM; (e) Natural light angle; (f) Backlight angle (g) Original figure; (h) Horizontal flip; (i) Rotate at any angle; (j) Vertical flip; (k) Mosaic enhancement; (l) Histogram equilibrium.

# Based on the improved YOLOv5s model

Given that the topsoil stripping machine only needs to detect the number of FUM, it is a single-class detection. YOLOv5 is a single-stage detection model with few parameters and fast detection speed and is widely used in actual agricultural operations (*Qanouni et al., 2025;*). To improve detection speed and accuracy, this study selects the YOLOv5s model, which performs well in terms of speed and accuracy, on the basis of the compatibility of the actual deployed hardware edge computing device Jetson Nano and the image features of the detection objects.

In view of the small target size and complex background of FUM, the detection accuracy and speed are improved by optimizing the network structure and introducing an attention mechanism. The Swin Transformer v2 attention module is introduced to enhance the modeling ability of local and global features. The ACON activation function is adopted to enhance the network's nonlinear expression capability (*Zhaoet al., 2023;*). The improved algorithm is referred to as YOLOv5s-Swin Transformer v2-ACON (abbreviated as YOLOv5s-SA algorithm), and its algorithm structure is shown in Fig. 6.

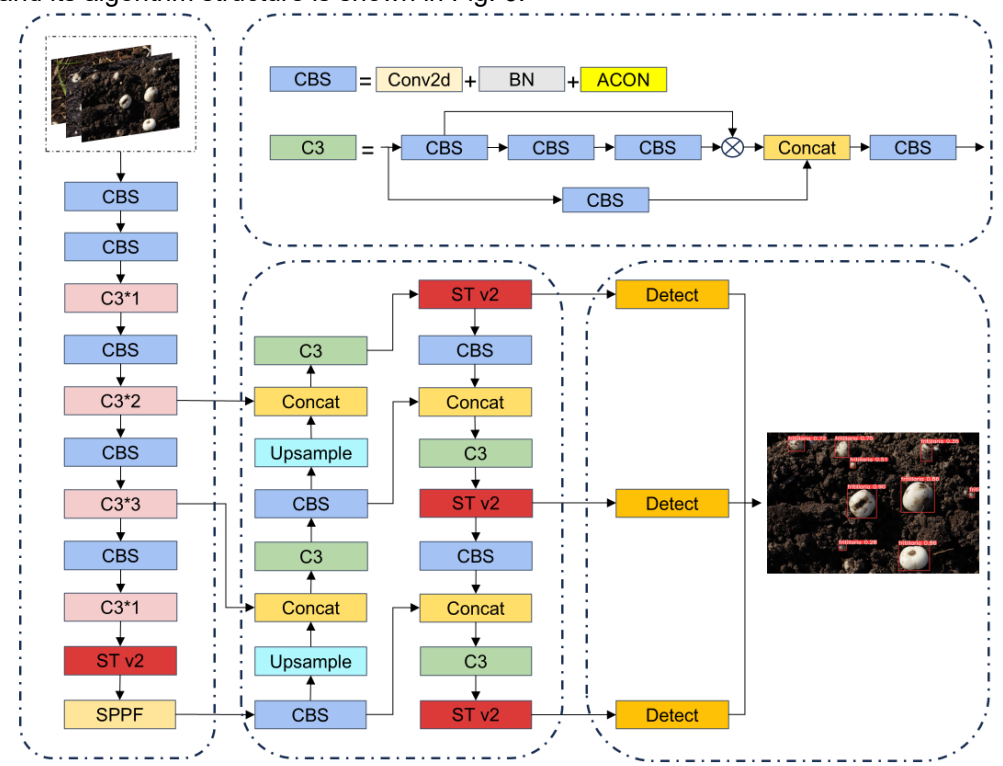


Fig. 6 – YOLOv5s-SA structure diagram

The hyperparameter settings for the algorithm training after pretraining are as follows: Ir0, 0.01; momentum, 0.937; weight\_decay, 0.0005; epochs, 300; batch size, 32. Under the same environmental conditions and parameter settings, the YOLOv5s and YOLOv5s-SA network models were trained separately. The results showed that the average mean precision of the YOLOv5s-SA model was 4 percentage points higher than that of the original model. The improved YOLOv5s-SA model outperformed the YOLOv5s model in terms of mAP, F1 score (F1), and precision (P). with mAP reaching 96.6%. The results of the field tests are shown in Fig. 7.

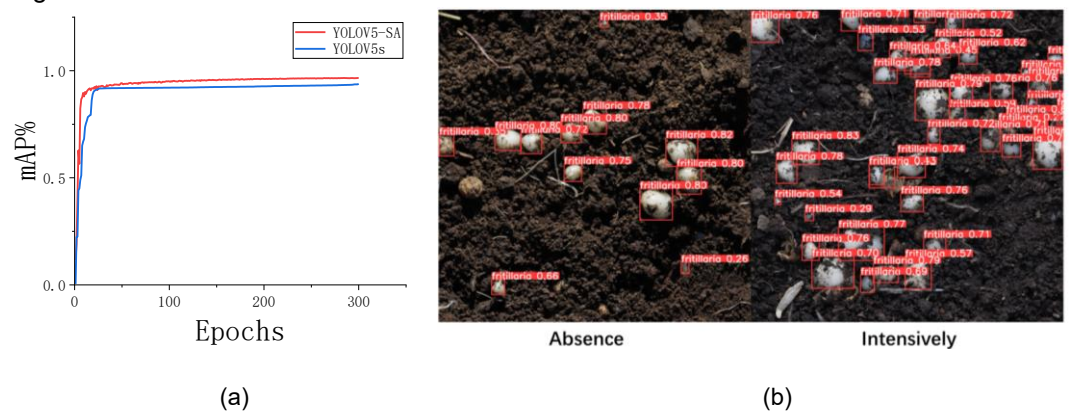
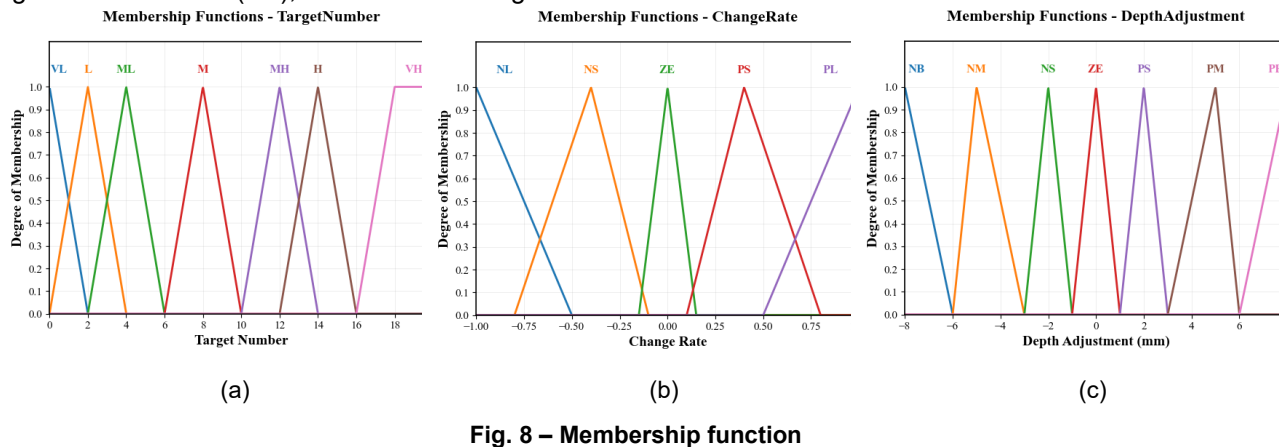


Fig. 7 – Comparison of model detection performance
(a) mAP (b) Test results for different FUM densities

# Fuzzy control algorithm design

The fuzzy controller takes two parameters from the image recognition system—FUM exposure number N and short-term change rate  $\Delta N$ —as inputs, and outputs the servo electric cylinder adjustment  $\Delta d$  based on fuzzy rules derived from manual operation experience. It consists of fuzzification, rule base, inference, and defuzzification modules, establishing a fuzzy mapping between input and output (*Ban et al., 2024;*). Fuzzification converts exact values into fuzzy variables by discretizing continuous data into fuzzy sets. Considering FUM planting density, vision frame rate, and operating speed, the domain of N is set to [0, 20] plants,  $\Delta N$  to [-1, 1], and  $\Delta d$  to [-8 mm, 8 mm]. Triangular membership functions are adopted for all variables due to their sensitivity and computational simplicity. N is divided into seven subsets (VL, L, ML, M, MH, H, VH),  $\Delta N$  into five subsets (NL, NS, ZE, PS, PL), and  $\Delta d$  into seven subsets from significant increase (NB) to significant decrease (PB), as illustrated in Fig. 8.



The rule library is the basis for fuzzy controllers to perform logical reasoning and is usually derived from human operational experience and experimental feedback. For fuzzy controllers with two inputs and one output, the fuzzy reasoning rules are described as follows:

If (N is A) and ( $\Delta$ N is B), then ( $\Delta$ d is C).

Among them, A, B, and C represent the detection quantity, short-term change rate, and fuzzy terms of the output variable, respectively. On the basis of the manual operation experience of the topsoil stripping machine, 35 control rules were established, as shown in Table 2. Given that the fuzzy control output is a fuzzy quantity, it cannot be directly used to drive the servo electric cylinder movement. Therefore, defuzzification must be performed using the center of gravity method to obtain the corresponding continuous quantity  $\Delta d$ , which serves as the displacement adjustment command for the servo electric cylinder controller.

Table 2

Rules	Library
-------	---------

NI	ΔΝ				
N	NL	NS	ZE	PS	PL
VL	PB	PM	PM	PS	PS
L	PM	PS	PS	ZE	PS
ML	PS	PS	ZE	PM	PM
M	ZE	ZE	ZE	ZE	ZE
MH	NS	NS	NB	NM	NB
Н	NM	NM	NM	NB	NB
VH	NB	NB	NB	NB	NB

## **Control strategy**

With the image processing results used as feedback and the extension length of the servo electric cylinder used as the control variable, a closed-loop control system for digging depth is formed. The system control flow chart is shown in Fig. 9.

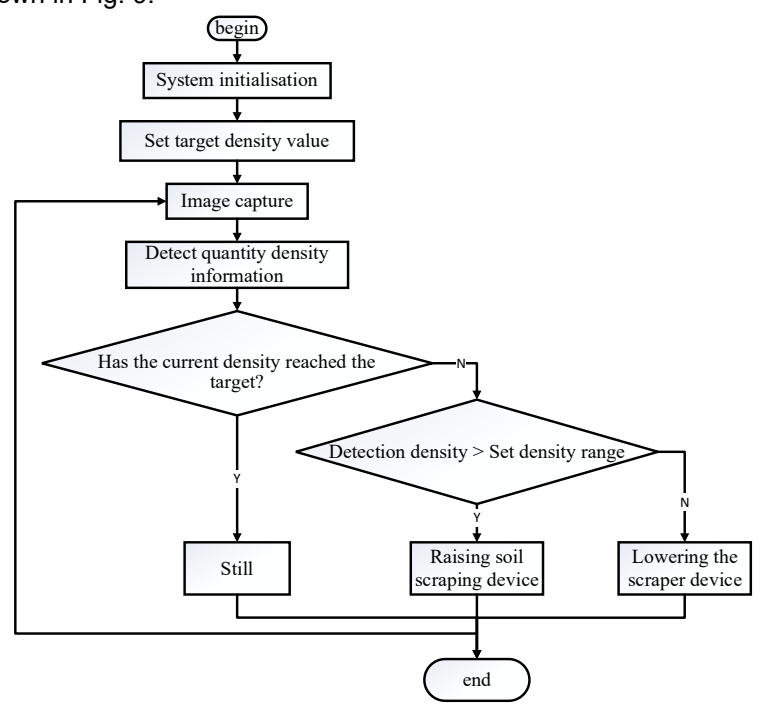


Fig. 9 - System control flowchart

To avoid undercompensation caused by "entering the next frame determination before the soil scraping plate is in place," a time—speed constraint model for the camera guidance control system will be established, and the theoretical upper limit for the maximum travel speed will be provided.

The effective visual length obtained by the current camera each time is  $L_{var}$ . When the work platform moves forward at a speed of v, the time required for one complete coverage is:

$$T = \frac{L_{var}}{v} \tag{1}$$

Therefore, the control cycle should meet the following requirements to ensure that the overall adjustment response time  $t_{sys}$  completes one control cycle:

$$T \geq t_{sys} \tag{2}$$

Therefore, from Equations (1) and (2), the time constraint for the travel speed can be obtained:

$$v \le \frac{L_{var}}{t_{svs}} \tag{3}$$

When the maximum allowable depth adjustment per cycle is  $\Delta d_{max}$ , and considering the redundancy introduced by signal processing and uncertainty, the effective action time  $t_{eff} = \eta T \ (0 < \eta < 1)$  is defined as the safety factor. Therefore, the minimum speed required for the servo electric cylinder is:

$$v_c = \frac{\Delta d_{max}}{\eta T} \tag{4}$$

By substituting (1) into (4), the linear relationship between the servo electric cylinder speed and the travel speed is obtained:

$$v_c = \frac{\Delta d_{max} v}{\eta L_{var}} \tag{5}$$

Therefore, the basic constraint equations can be obtained by combining Equations (1) and (4).

$$v_c T = \frac{\Delta d_{max}}{\eta} \tag{6}$$

Given that the system must simultaneously satisfy two constraints, namely, the control cycle and the servo electric cylinder capacity:

Therefore, by substituting (1) and (5) into Equation (7), the comprehensive upper limit of the travel speed is obtained:

$$v \leq min\left(\frac{L_{var}}{t_{sys}}, \frac{v_{c, max}\eta L_{var}}{\Delta d_{max}}\right)$$
(8)

Therefore, as shown by Equation (8), increasing  $L_{var}$  or reducing  $\Delta d_{max}$  helps to relax the two types of constraints. While increasing the safety factor  $\eta$  can reduce the servo electric cylinder speed requirement, it also compresses the effective action time, necessitating a comprehensive trade-off. Therefore, the current travel speed of the FUM topsoil stripper is 0.6 km/h, the servo electric cylinder speed is 50 mm/s, the camera field of view length is 0.2 m, and the maximum depth adjustment is 8 mm, which meets the system working requirements. From this, the control cycle T is determined to be 1.2 s.

The PyQt interface designed is shown in Fig. 10. The interface can be used to adjust various parameters via the touch screen before work begins.

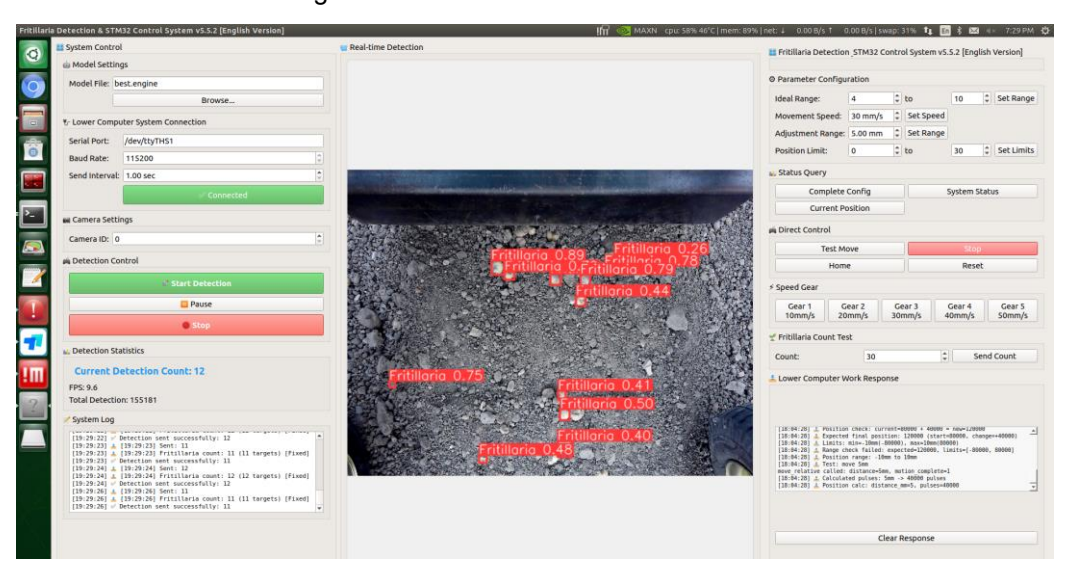


Fig. 10 – Upper computer monitoring interface

#### **RESULTS**

#### Deployment of object detection algorithms and RT acceleration

To improve the inference efficiency of the model on edge AI device platforms, an intermediate model in ONNX format was adopted, and the NVIDIA TensorRT toolchain was used to compile and accelerate the model on the Jetson Nano platform. The .pt files exported after training the YOLOv5 series models are large and consume high inference resources, which will significantly affect system real-time performance if deployed directly.

By converting to the TensorRT engine format, graph computation optimization and convolution/activation fusion can be achieved, thereby reducing model load and improving execution efficiency (*Lv et al., 2025*). In this experiment, the input image resolution was set to 640×640, and 300 frames of images were processed continuously. The system clock was recorded at the start and end of model inference, and the average inference time was calculated. To eliminate external interference, the graphical interface and disk write operations were disabled during testing to ensure exclusive access to GPU resources. The average detection time for each model on different platforms and inference frameworks is shown in Table 3.

Table 3

moust detection time			
model	t1 (s)	t2 (s)	t3 (s)
YOLOv5s	0.033	0.184	0.117
YOLOv5s-SA	0.021	0.118	0.077

Model detection time

<sup>\*</sup> Note: t1 represents the detection time for inference on a PC; t2 represents the detection time for inference on the original .pt model on Jetson Nano; t3 represents the detection time for inference on the engine model using TensorRT on Jetson Nano.

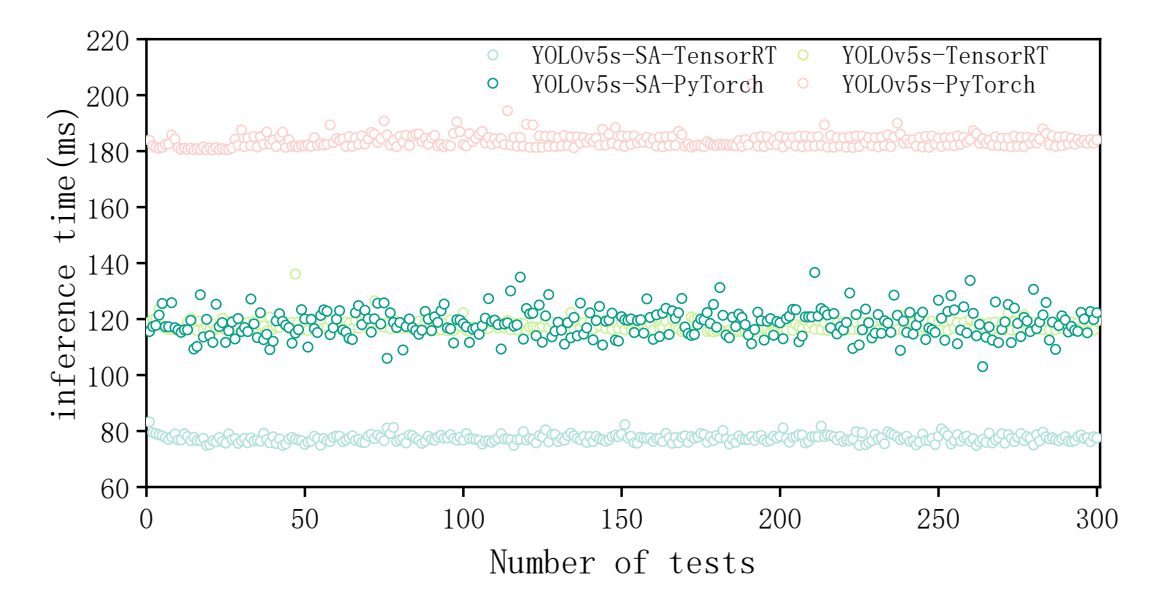


Fig. 11 - Time required for image processing of 300 frames of FUM

# System response testing

To evaluate the real-time performance of deep regulation, the total system response time  $t_{sys}$  is divided into image processing time  $t_3$ , control signal transmission time  $t_4$ , and actuator response time  $t_5$ , which are related as follows:

$$t_{SVS} = t_3 + t_4 + t_5 \tag{9}$$

Image processing time  $t_3$ : Deploying the lightweight YOLOv5-SA model on Jetson Nano and performing inference with RT acceleration. This process was measured in Section 3.1 and took 0.077 seconds.

$$t_3 = \frac{1}{N} \sum_{i=1}^{N} (t_{i,end} - t_{i,start})$$
 (10)

Decision signal transmission time  $t_4$ : A 100 MHz oscilloscope was used to simultaneously monitor the rising edges of the Jetson Nano GPIO trigger signal and the STM32 PWM output signal, and the delay was calculated. The measured time for this process was 0.0058 seconds.

$$t_4 = t_{PWM_{rise}} - t_{GPIO_{rise}} \tag{11}$$

Actuator response time  $t_5$ : Fill the test soil scraping mechanism with 100 mm thick soil, and move the test bench between the soil ridges at a typical speed of 0.6 km/h for removing topsoil using FUM. Use computer monitoring software to control the extension and retraction of the soil scraping plate at different soil depths, and use a single-chip microcomputer to collect the number of opposite feedbacks from the electric cylinder photoelectric encoder Z to determine whether the electric cylinder is in the correct position. The response time was measured using the timer of the single-chip microcomputer and the number of external interrupts. The timer of the single-chip microcomputer was set to a timing cycle of 5 ms. The response time was used to determine the change in the maximum adjustment length of the electric cylinder at different soil depths. Since no FUM detection crops were planted on the soil ridge surface, the camera captured zero recognition information. Based on the set fuzzy control algorithm, the maximum elongation under single control was determined to be 8 mm.

Displacement response time at different soil depths

l able 4

Soil depth / mm	Soil response time averages / ms	Average soil-free response time / ms
50	176	
55	174	
60	172	
65	178	164
70	181	
75	177	
80	180	

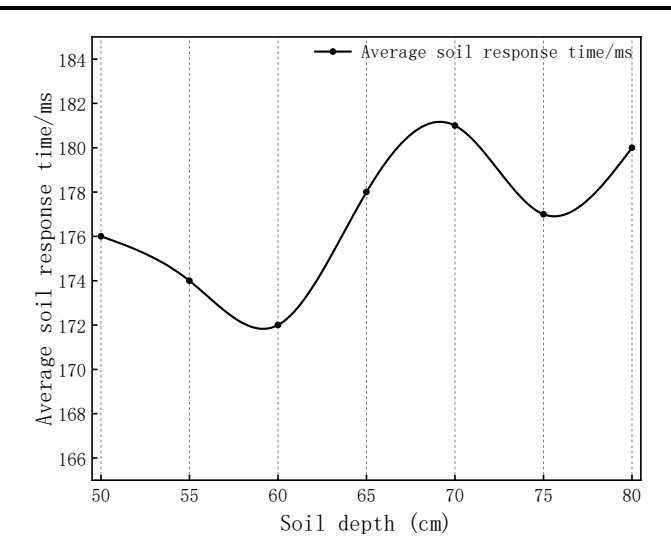


Fig. 12 - Response time at different soil depths

The results showed that soil filling had little effect on response time (average difference of 13 ms), and the average response time under soil filling was calculated to be 0.177 s.

Therefore,  $t_{sys}$  is the total time for the stripping response (0.077 s + 0.0058 s + 0.177 s) s. Finally, the time after the topsoil stripping response is approximately 0.26 s relative to the electrical signal.

The servo electric cylinder can achieve an operating speed of up to 50 mm/s, with a maximum stroke of 8 mm in 0.26 seconds; the topsoil stripper can advance approximately 0.043 m in 0.26 seconds at a speed of 0.6 km/h. In contrast, topsoil strippers use traditional air springs and hydraulic control systems, which require the hydraulic pump and air pump to be started before operation. The depth of soil scraping is adjusted by switching the electromagnetic valve on and off. The start-up and operation time is significantly longer than 0.26 seconds. Therefore, compared with the other two control methods, the servo electric cylinder control system has lower system delay in soil scraping adjustment and can alleviate the soil scraping lag problem to a certain extent.

#### **Motion error test**

In the topsoil stripping system, vertically mounted servo electric cylinders drive the scraper plate to adjust stripping depth, and depth errors directly affect removal quality. To evaluate actuator accuracy, a motion error test was conducted (Fig. 13). The test simulated field operation indoors by inserting the scraper plate into a soil ridge and performing reciprocating movements.

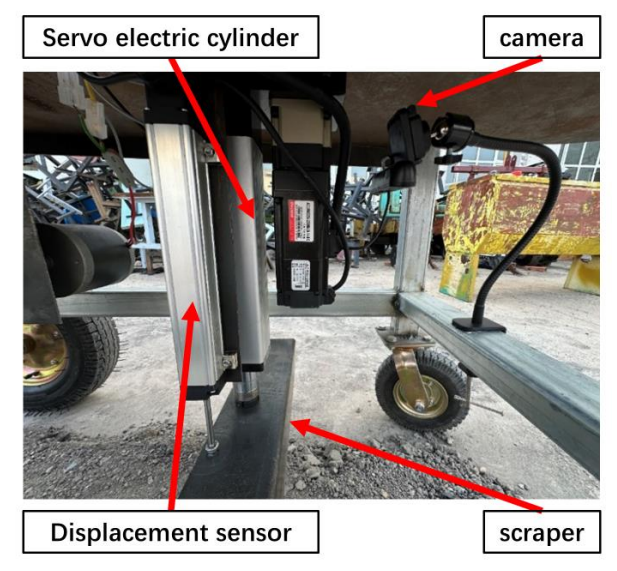


Fig. 13 - Installation diagram of displacement sensor and servo electric cylinder

Motion commands were sent from a Jetson Nano to a microcontroller, with test depths set at 50, 60, 70, and 80 mm—covering the typical FUM stripping range (50–80 mm). The scraper was retracted by 5 mm per step until returning to the initial position. Each setting was tested five times in both extension and retraction directions, and displacement sensor readings were recorded to calculate average motion error. Test results are summarized in Table 5.

Results of motion error tests

Table 5

Target displacement/mm	Average displacement/mm	5 mm retractions	Average error/mm
50	50.02	10	0.02
55	54.93	11	0.07
60	59.45	12	0.55
65	65.31	13	0.31
70	70.06	14	0.06
75	74.88	15	0.12
80	80.61	16	0.61

As shown in the table, the maximum average error of the servo electric cylinder action is 0.61 mm, with an error not exceeding 1 mm, thus meeting the requirements for precise stripping tests. Analysis of the mechanical structure of the servo electric cylinder revealed that the motion error was mainly caused by mechanical clearance between the gear and the lead screw during movement. The main causes of mechanical clearance are machining errors and installation errors. Improvements need to be made during the manufacturing process of the servo electric cylinder to reduce the error caused by clearance.

# Topsoil stripping performance test

To evaluate the system's performance in controlling topsoil stripping under simulated field conditions, a 12 m × 0.4 m × 0.1 m soil ridge stripping test platform was constructed within the Engineering College of the Ba Yi Agricultural University in Heilongjiang Province (Fig. 14).



(a)



(b)

Fig. 14 – Soil ridge simulation experiment
(a) FUM laid out (b) Experimental scenario diagram

FUM sample plants were simulated buried in three layers, buried at depths of 50, 60, and 70 mm, respectively. The size of each layer of sample plants was randomly arranged, and the ideal density range of FUM in a single operation was set to 6–10 plants. The travel speed was 0.6 km/h, the servo electric cylinder speed was 50 mm/s, and the machine walked 0.2 m each time. The servo electric cylinder output displacement was recorded using a displacement sensor.

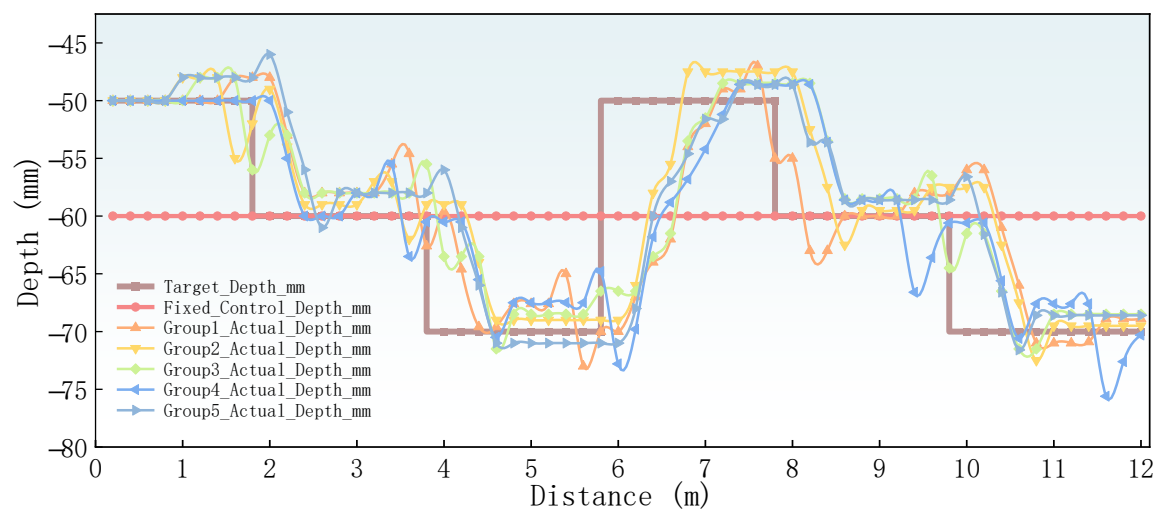


Fig. 15 – Changes in working depth during automatic control system operation with the same burial depth for both closing and opening operations

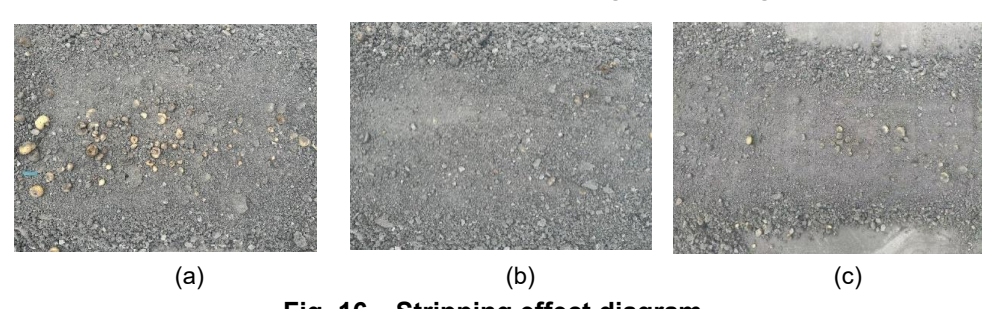


Fig. 16 – Stripping effect diagram
(a) Excessive stripping (b) Insufficient stripping (c) Ideal separation

#### CONCLUSIONS

This study addresses the current issues in the harvesting of FUM, such as the lack of intelligent assurance of a constant digging depth, reliance on manual adjustment, low control accuracy, and response lag. A machine-vision-based automatic control system for topsoil stripping was designed and implemented. The system integrates an improved YOLOv5 object detection algorithm and is deployed on the Jetson Nano edge AI computing platform and servo electric cylinder actuators. Combined with a fuzzy control strategy, the system achieves real-time adaptive adjustment of the stripping depth.

The experimental results show that the proposed YOLOv5s-SA model achieves a mAP of 96.6% in FUM detection, which is 4 percentage points higher than the basic YOLOv5s. After acceleration with TensorRT, the model achieves an inference time of 0.077 seconds on the Jetson Nano platform. In a simulated test platform, the control system reduces the average depth error from 6.67 mm under fixed control to 3.72 mm, representing a 44.1% improvement in error reduction; the average ideal separation rate improves to 54.96%, an increase of 21.66% compared with fixed control. The system's total response time is approximately 0.26 seconds, demonstrating excellent control accuracy and responsiveness, outperforming traditional hydraulic or pneumatic regulation methods.

#### **ACKNOWLEDGEMENT**

This study was funded by the Education Department of Heilongjiang Province for the Heilongjiang Province "Double First-Class" Discipline Collaborative Innovation Achievement Project (Grant No. LJGXCG2023-050), the Education Department of Heilongjiang Province for the Heilongjiang Province "Double First-Class" Discipline Collaborative Innovation Achievement Project (Grant No. LJGXCG2022-112), and the University Oriented Talent Cultivation Research Start-up Project (Grant No. XDB202401).

#### **REFERENCES**

- [1] An, Y.-I., Wei, W.-I., Guo, D.-a. (2024). Application of analytical technologies in the discrimination and authentication of herbs from *Fritillaria*: a review. *Critical Reviews in Analytical Chemistry*, Vol. 54(6), pp.1775–1796, United Kingdom.
- [2] Ban, C., Chi, R., Huang, X., Dong, N., Su, T., Sun, X. (2024). Design and experiment of corn-spraying robot with LiDAR navigation (基于激光雷达导航的玉米喷药机器人设计与试验). *Nongye Jixie Xuebao / Transactions of the Chinese Society of Agricultural Machinery*, Vol. 55(S2), pp. 200–209, Beijing/China.
- [3] Dai, H., Dou, Y., Wang, G., Zhu, Z. (2019). An automatic excavation depth control system for semi-feeding four-row peanut combine harvester. [C]// 2019 11th International Conference on Intelligent Human-Machine Systems and Cybernetics (IHMSC), Vol. 1, pp. 184–187, United States.
- [4] Ding, A., Peng, B., Yang, K., Zhang, Y., Yang, X., Zou, X., Zhu, Z. (2022). Design of a machine vision-based automatic digging depth control system for garlic combine harvester. *Agriculture*, Vol. 12(12), pp. 2119, Switzerland.
- [5] Jiao, N., Song, X., Song, R., Yin, D., Deng, X. (2022). Diversity and structure of the microbial community in rhizosphere soil of *Fritillaria ussuriensis* at different health levels. *PeerJ*, Vol. 10, pp. e12778, United States.
- [6] Li, F., Lei, W., Li, J., Wang, X., Su, J., Sahati, T., Aierkenjiang, X., Tian, R., Zhou, W., Zhang, J. (2025). A dual-technology approach: Handheld NIR spectrometer and CNN for *Fritillaria* spp. quality control. *Foods*, Vol. 14(11), pp. 1907, Switzerland.
- [7] Li, S., Hu, H., Wu, L. (2022). Optimum design and simulation analysis of drum screen for *Fritillaria* harvester. *Journal of Agricultural Mechanization Research*, Vol. 11, pp. 46–50, Heilongjiang/China.
- [8] Lv, Z., Yang, S., Ma, S., Wang, Q., Sun, J., Du, L., Han, J., Guo, Y., Zhang, H. (2025). Efficient deployment of peanut leaf disease detection models on edge Al devices. *Agriculture*, Vol. 15(3), pp. 332, Switzerland.
- [9] Qanouni, F., El Massari, H., Gherabi, N., El-Badaoui, M. (2025). SSAM\_YOLOv5: YOLOv5 enhancement for real-time detection of small road signs. *Digital*, Vol. 5(3), pp. 30, Switzerland.
- [10] Sang, X., Zhang, K., Yang, L., Zhang, D., Cui, T., He, X., Qi, H., Mou, J. (2024). Design and experiment of a stereoscopic vision-based system for seeding depth consistency adjustment. *Computers and Electronics in Agriculture*, Vol. 225, pp. 109345, Netherlands.
- [11] Shi, M., Li, Y., Pan, Y., Lu, L., Wei, J. (2024). Design of an adaptive height control system for sugarcane harvester header. *Agronomy*, Vol. 14(8), pp. 1644, Switzerland.
- [12] Song, H., Shang, Y., He, D. (2023). Review on deep learning technology for fruit target recognition (果

- 实目标深度学习识别技术研究进展). Nongye Jixie Xuebao / Transactions of the Chinese Society of Agricultural Machinery, Vol. 54(1), Beijing/China.
- [13] Song, J., Qiu, S., Wang, X. (2015). Design and test on 4B-1200 type bulbus *Fritillariae ussuriensis* medicinal material harvester (4B-1200 型平贝母药材收获机的设计与试验). *Transactions of the Chinese Society of Agricultural Engineering*, Vol. 31(8), pp. 34–41, Beijing/China.
- [14] Song, J., Liu, L., Wang, M., Zhang, J. (2017). Improved design and test of 4B-1200 type *Bulbus Fritillariae Ussuriensis* medicinal materials harvester (4B-1200 型平贝母药材收获机的改进设计与试验). *Transactions of the Chinese Society of Agricultural Engineering*, Vol. 33(1), pp. 45–51, Beijing/China.
- [15] Song, J., Tian, S., Wang, Y., Han, X., Wang, M., Sun, X., Yi, S. (2023). Analysis of impact and absorbed energy of *Fritillaria ussuriensis* Maxim during drum screening and its effect on impact damage. *Computers and Electronics in Agriculture*, Vol. 215, pp. 108368, Netherlands.
- [16] Tao, L., Li, N., Liu, C., Zhu, Z., Zhou, J., Zhang, H. (2021). Development of automatic depth control system employed in potato harvester (薯类收获机挖掘深度自动控制系统设计与试验). *Nongye Jixie Xuebao / Transactions of the Chinese Society of Agricultural Machinery*, Vol. 52(12), Beijing/China.
- [17] Wang, Y., Li, H., Feng, X. (2025). Research progress on agricultural equipments for precision planting and harvesting. *Agriculture*, Vol. 15(14), pp. 1513, Switzerland.
- [18] Xiong, C., Zhou, D., Deng, G., Li, G., Cui, Z., He, F., Li, L. (2022). Design and test of automatic control system for excavation depth of vibrating chain cassava harvester (振动链式木薯收获机挖掘深度自动控制系统设计与测试). *J. Huazhong Agric. Univ / Journal of Huazhong Agricultural University*, Vol. 41(2), pp. 217–226, Hubei/China.
- [19] Yang, Z., Shah, S. F. A., Huang, X., Wei, L., Zhong, Y., Shi, X., Wu, X., Gan, C., Wang, Z., Yang, C. (2025). A multi-level study on the anti-lung cancer mechanism of peiminine, a key component of *Fritillaria ussuriensis* Maxim.: Integrating quality analysis, network pharmacology, bioinformatics analysis, and experimental validation. *International Journal of Molecular Sciences*, Vol. 26(8), pp. 3506, Switzerland.
- [20] You, Z., Wu, H., Hu, Z., Peng, B. (2015). Fuzzy control on digging depth of 4HLB-2 peanut harvester (花生收获机4HLB-2型挖掘深度的模糊控制). *J. Northwest A&F Univ (Nat. Sci. Ed) / Journal of Northwest A&F University, Natural Science Edition*, Vol. 43, pp. 221–227, Shaanxi/China.
- [21] Zhao, W., Tian, S., Zhang, Q., Wang, Y., Wang, S., Song, J. (2023). Detection model of *Fritillaria ussuriensis* Maxim based on improved YOLOv5 (基于改进 YOLOv5 的平贝母检测模型). *Journal of Guangxi Normal University Natural Science Edition*, Vol. 41(6), pp. 22–32, Guangxi/China.